Cold spells induced by slow and amplified atmospheric waves

Morteza Babaei[1*], Rune Grand Graversen[1,2], Johannes Patrick Stoll[2], and Jakub Petříček[1]

[1]Department of Physics and Technology, University of Tromsø, Tromsø, Norway
[2]Norwegian Meteorological Institute, Tromsø, Norway

Correspondence: Morteza Babaei (morteza.babaei@uit.no)

Abstract. Cold spells in the Northern Hemisphere mid-latitudes have been linked to ~~planetary~~ Rossby waves. Yet the mechanisms by which these waves impact cold-spell formation remain unclear. Here we develop novel metrics to separately measure the amplitude and speed of ridges and troughs, examining the behavior of ~~planetary~~ Rossby waves during winter cold spells. Our findings indicate that while ~~the planetary waves~~ ridges and troughs across the entire mid-latitudes experience significant changes during cold spells, ~~local wave dynamics~~ the local ridge and trough near the cold spell's location play a major role in ~~developing~~ the development of these events. The nearest upstream ridge and downstream trough of the cold-spell region are located in a way that facilitates development of the extreme cold anomaly. This ridge and trough amplify and slow, enhancing and prolonging southward advection of cold air from the Arctic into the cold-spell region. The slow and amplified upstream ridge and downstream trough occur several days before the region's minimum temperature, suggesting these local wave anomalies induce cold-spell formation.

1 Introduction

~~The large-scale mid-latitude waves play a crucial role in shaping weather patterns in~~ High-amplitude quasi-stationary Rossby waves may generate extreme weather events (e.g., Hoskins and Woollings, 2015; Fragkoulidis and Wirth, 2020; White et al., 2022), and increase in temperature extremes in the mid-latitudes ~~(?). In 1937, Bjerknes provided pioneering work on a dynamical explanation for the movement of mid-latitude waves (?). His elucidation on the movement of zonal pressure disturbances inspired Rossby to provide a mathematical description of the atmosphere's planetary wave behavior, which we now refer to as Rossby waves (?). Rossby waves are large-scale atmospheric phenomena characterized by meandering patterns in winds, primarily influenced by pressure differences and the Earth's rotation and the resulting variation of the Coriolis effect with latitude (?). Slow-moving (quasi-stationary) Rossby waves can be associated with strong waveguide occurrences (?) and atmospheric blocking (???).~~

~~The ability of high-amplitude quasi-stationary Rossby waves to generate extreme weather events has been acknowledged (e.g., ??)~~is argued to be linked to increased upper-atmosphere waviness (e.g., Fragkoulidis et al., 2018). An increase in meridional amplitude of Rossby waves may enhance the meridional exchange of warm and cold air, leading to the advection of cold air ~~further~~ to the south and warm air to the north ~~(??).~~ (Zschenderlein et al., 2018; Jolly et al., 2021). Some studies link extreme temperatures to a significant amplified circumglobal waviness based on wave amplitudes of individual wave numbers (Petoukhov et al., 2013; Screen and Simmonds, 2014), while others assert a robust correlation between local waviness and

temperature extremes (Röthlisberger et al., 2016; Fragkoulidis et al., 2018; Fragkoulidis and Wirth, 2020). Studies based on the amplified circumglobal waviness argued that free-traveling synoptic waves of some specific wave numbers (6, 7, or 8) may be trapped within the midlatitude waveguide leading to extreme temperature events (Petoukhov et al., 2013; Kornhuber et al., 2017) , whereas others caution against overemphasizing the significance of circumglobal waviness, suggesting that local climatic factors may play a more critical role in influencing temperature extremes (Teng and Branstator, 2019).

Slow movement of Rossby waves may also lead to weather persistence, ~~enhancing the probability of development of~~ for instance in terms of blocking, which may develop into extreme weather events, such as floods, droughts, heat waves, and cold spells ~~(????). A negatively tilted trough, extending from northwest to southeast up through the troposphere, generated through strengthening the wind shear, is another type of atmospheric wave that may generate circumstances favorable for severe weather (?). Therefore, to understand the formation of extreme weather, it is critical to take the dynamics of Rossby waves into account~~(Francis and Vavrus, 2012; Pfleiderer and Coumou, 2018; Riboldi et al., 2020; Jolly et al., 2021; Wicker et al., 2024). Extreme rainfall over Eastern Australia has been linked to slow-moving upper-level low-pressure systems (Barnes et al., 2023; Reid et al., 2025; Vrie , and it is argued that slow propagation of atmospheric blocking, identified using a blocking cell-tracking algorithm, lead to significant surface temperature anomalies (van Mourik et al., 2025). The propagation speed of atmospheric blocking can impact the upstream and downstream of the block, in the way that rapidly westward-moving blocks lead to less persistent cold events in the upstream of the block, while slower westward-moving or quasi-stationary blocks lead to strong cold anomalies in the downstream of the block (Chen and Luo, 2017; Yao et al., 2017).

The frequency of extreme events has risen in recent decades due to anthropogenic warming ~~(IPCC; ?), and they~~ (IPCC; Seneviratne et al., , and these events are likely to become more intense and break the previous extreme records by a large margin in the following decades ~~(?). One such recent catastrophe is the late October 2024 flash floods in Spain, which caused 224 fatalities and substantial economic damage (??). In 2024, 27 extreme weather events, including two winter storm events, each with losses exceeding one billion dollars, affect the United States. On top of the significant economic damage of these events, they caused the deaths of 568 people (?). In~~ (Fischer et al., 2021). In addition, despite the warming Earth, cold spells ~~and heavy snowfalls across~~ in some regions of the Northern Hemisphere have ~~increased (e.g., ???). On January 13, 2024, Billings, Montana, recorded its lowest temperature ever measured (?), during the warmest winter ever recorded in the continental United States (?). Such unusually low temperatures also occur in Scandinavia recently. On January 3, 2024, the Swedish village of Kvikkjokk recorded Sweden's lowest January temperature in 25 years (?)~~recently increased (e.g., Cohen et al., 2021, 2024), although, in general, cold spells are projected to become less frequent by the end of the century (IPCC; Seneviratne et al., 2021) , and the likelihood of experiencing the strongest historical extreme cold spell events is expected to diminish (Ribes et al., 2025) .

~~It has been suggested that the increases in severe events~~Increases in extreme event frequency, specifically cold spells, ~~are~~ have been linked to Arctic amplification (AA), a phenomenon by which the Arctic warms faster than the mid-latitudes ~~(e.g., ??)~~ (e.g., Francis and Vavrus, 2012; Cohen et al., 2014): the AA is weakening the jet stream, making the large-scale atmospheric waves more wavy ~~(???). In addition, Rossby waves~~ (Francis and Vavrus, 2012; Coumou et al., 2015; Stendel et al., 2021); in addition, AA causes Rossby waves to become more stationary, resulting in an increase in the frequency of extreme weather ~~(?)~~

(Francis and Vavrus, 2012). This hypothesis, however, has been questioned by several studies ~~(e.g., ????)~~(e.g., Barnes, 2013; Screen and Si
.

~~A recent study shows heat waves in some regions are associated with slow waves, whereas in other regions with fast waves~~ ~~(?)~~The dispute about the influence of the AA on planetary waves might stem from the sensitivity of waviness assessments to the applied metric (Geen et al., 2023), highlighting the need for improved and universal wave metric. Existing wave amplitude metrics, such as Rossby wave packets (e.g., Fragkoulidis et al., 2018; Röthlisberger et al., 2019), local jet waviness (e.g., Röthlisberger et al , and hemispheric variability (e.g., Petoukhov et al., 2013; Kornhuber et al., 2019), do not establish the role of the amplitude of each ridge and trough in temperature events. In addition, ~~it is argued high propagation speeds of atmospheric blocking, identified using a blocking cell-tracking algorithm, can lead to significant surface temperature anomalies (?). These findings emphasize inconsistency in our understanding of the role of large-scale circulation in mid-latitude extreme events across different regions~~as far as the authors know, the speed of local ridges and troughs and their role in extreme events have not earlier been quantified. Some studies estimate atmospheric phase propagation by following grid points using lag-correlation in different bandpass-filtered geopotential height maps, tracking the maximum positive correlation center (e.g., Blackmon et al., 1984; Takaya . Others derive phase-speed spectra for each zonal wavenumber by performing a space–time spectral decomposition of upper-tropospheric winds along latitude circles (e.g., Randel and Held, 1991; Domeisen et al., 2018; Riboldi et al., 2020). A local approach is also used to estimate the speed of Rossby wave packets (e.g., Fragkoulidis and Wirth, 2020; Fragkoulidis, 2022). Here, we ~~attempt to analyze the large-scale structure of Rossby waves during cold spells~~ aim to explore the linkage between cold spells and the amplitude and speed of each ridge and trough. Cold spells are particularly of interest in the context of Rossby waves because these cold extremes are argued to be primarily driven by the large-scale advection of cold air from higher latitudes ~~(?)~~ (Bieli et al., 2015; Tuel and Martius, 2024). Hence, this study further investigates the role of ~~Rossby waves~~ individual ridges and troughs in causing cold spells.

2 Methods

In this study, we used the European Centre for Medium-Range Weather Forecasts (ECMWF) analysis 5th Generation (ERA5) dataset with a horizontal resolution of 0.25°×0.25° ~~(?)~~ (Hersbach et al., 2020) for the period 1978-2024. The study is for the winter season (December-January-February) and the satellite era. Minimum daily temperature and daily average temperature are obtained based on hourly ERA5 data. Additionally, 3-hourly geopotential height data at 300 hPa, 500 hPa, and 850 hPa are utilized.

2.1 ~~Study regions selectionIt may appear attractive to adopt the climate reference regions suggested by the IPCC (?) to align the boundaries of our study regions. However, cold spells manifest spatially differently than do the seasonal mean temperature patterns used in identifying the IPCC climate reference regions. For instance, in January 2024, cold spells occurred in Scandinavia, while there were no such events in the British Isles (?). The IPCC classifies all these countries in a single region, while in our study they are classified in two regions. In addition, the interest here is to select regions in which cold~~ Cold spells~~are assumed to be originating from~~

To identify cold spells and their magnitudes, the cold wave magnitude index daily (CWMId; Morlot et al., 2023) is applied at each horizontal grid point. The daily cold spells index is based on at least three consecutive days below a daily threshold, defined as the 90th percentile of anomalies relative to the climatology of minimum daily air temperature smoothed with a 31-day running mean filter. The climatology is based on the reference period 1981–2020. The background trend is small relative to the daily anomalies and we have checked that it does not affect the overall conclusions drawn in the paper (not shown).

2.2 Study regions selection

To select cold spell regions, we first identified historical extreme cold days on the hemispheric scale. To do so, a non-standardized version of the mid-latitude extreme (MEX; Riboldi et al., 2020) index is applied for land in four latitude bands (35-45°N, 45-55°N, 55-65°N, and entire mid-latitudes: 35-65°N). Dividing the mid-latitudes into three sub-bands enables an identification of extreme cold days in the lower, middle, and upper sections of the mid-latitudes. The MEX provides an overall measure of mid-latitude temperature daily variance by averaging over each grid point in the mid-latitudes the squared anomaly of the temperature. Here, "non-standardized" means the MEX index is used without subtracting its time-averaged mean and dividing by its standard deviation, as done in Coumou et al. (2014). The top 1% of daily MEX values—a criteria to classify cold extreme days—within all the winters during the period 1978-2024 yields 125, 117, 119, and 141 days for the bands 35-45°N, 45-55°N, 55-65°N, and 35-65°N, respectively. To identify the areas providing the largest cold anomaly contribution to the top 1 % MEX days of each latitude band, the CWMId (Fig. 1) and cold anomaly (supplementary Fig. S1) of the extreme cold days are calculated at each grid point in the mid-latitudes. Since these two diagnostics yield similar results, we focus on CWMId in the analysis.

Fig. 1 shows the composite of the geopotential height (gph) anomaly at 500 hPa and the cold-wave magnitude index for cold extreme days for each latitude band. For the top 1 % MEX days over the whole midlatitude (35-65°N; Fig. 1a), cold spells are more intense in the northwestern part of North America and northwestern Eurasia. The intensity decreases toward the south and east in both continents. The gph anomaly is positive over Greenland and the North Pacific Ocean, the two primary blocking regions (Barriopedro et al., 2006). Over the North Atlantic Ocean, a negative gph anomaly is encountered that may indicate the negative phase of the North Atlantic Oscillation (NAO) during these cold events, a phenomenon that promotes European winter cold spells (e.g., Hanna and Cropper, 2017; Vihma et al., 2020).

For the top 1 % MEX days over 35-45°N, little or no positive gph anomaly is encountered over Greenland, which is consistently associated with a weak intensity of CWMId over Europe (Fig. 1b). The main gph anomaly consists of a positive height anomaly over Alaska and a negative height anomaly downstream over West North America. Consistently, in this latitude band, CWMId is more pronounced over northwest North America, the central US, and Central Asia. Intense CWMId over Central Asia appears to differ from that of the central US, as it is likely not linked with higher latitudes, leading us to speculate that the cold spells in this region do not originate from Arctic cold air. ~~To select the regions for the study on cold spells, areas with the largest cold anomaly contribution to~~ Therefore, this region is not included in our study.

For the top 1 % MEX days over 45-55°N, in contrast to 35-45°N, there is a strong positive gph anomaly upstream of Europe, centered over Iceland, while the positive gph anomaly is weak upstream of North America (Fig. 1c). For this latitude band, the ~~historical extreme cold days on the hemispheric scale are chosen (see the supplementary information).~~ CWMId is strong over the middle and east of Europe and over the west of Canada. For the top 1 % MEX days over 55-65°N, CWMId is stronger at higher latitudes, encompassing Scandinavia, the west of Canada, and Northern Siberia (Fig. 1d). For this latitude band, there are two strong positive gph anomaly centers over Baffin Bay and the Bering Sea. The top 1 % MEX over the 45-55°N and 55-65°N, similar to MEX across the entire midlatitude, exhibits a negative gph anomaly over the North Atlantic Ocean.

Based on the results of the composite of days with the top 1 % MEX over these four latitude bands, 9 regions are selected for the study of the impact of large-scale upper atmospheric circulation on cold spells, shown as hatched areas in Fig. 2. The regions include Northwest Canada (R01), Northwest US and Southwest Canada (R02), Central US (R03), British Isles (R04), Scandinavia (R05), Europe (R06), Northwest Russia (R07), Southwest Russia (R08), and Northern Siberia (R09).

2.3 ~~Cold spells~~

~~To identify cold spells and their magnitudes, the cold wave magnitude index daily (CWMId; **?**) is applied at each horizontal grid point. The daily cold spells index is based on at least three consecutive days below a daily threshold, defined as the 90th percentile of anomalies relative to the climatology of minimum daily air temperature smoothed with a 31-day running mean filter. The climatology is based on the reference period 1981–2020. The background trend is small relative to the daily anomalies and we have checked that it does not affect the overall conclusions drawn in the paper (not shown).~~ If 50 % or more of the grid points within each region experience cold spells on a given day, it is considered a cold spell day in that region. Applying grid-point thresholds between 20 percent and 70 percent are also tested to ensure that the drawn overall conclusions remain unchanged for an altered threshold. The number of days with 50% or more of the grid points experiencing cold spells in each region, as based on the CWMId, is 239, 184, 164, 157, 170, 171, 195, 150, and 152, respectively, for R01 to R09.

2.3 ~~Wave speed~~Significant test

To test the null hypothesis that anomalies associated with the cold spells are zero, a Monte Carlo simulation with random samples is employed. Specifically, the average number of cold spell days across each region is compared with the average of an equivalent number of randomly selected days. Instead of selecting random days from the entire winter season, the selection is weighted based on the frequency distribution through the season of cold spell days, since cold spells appear to occur more

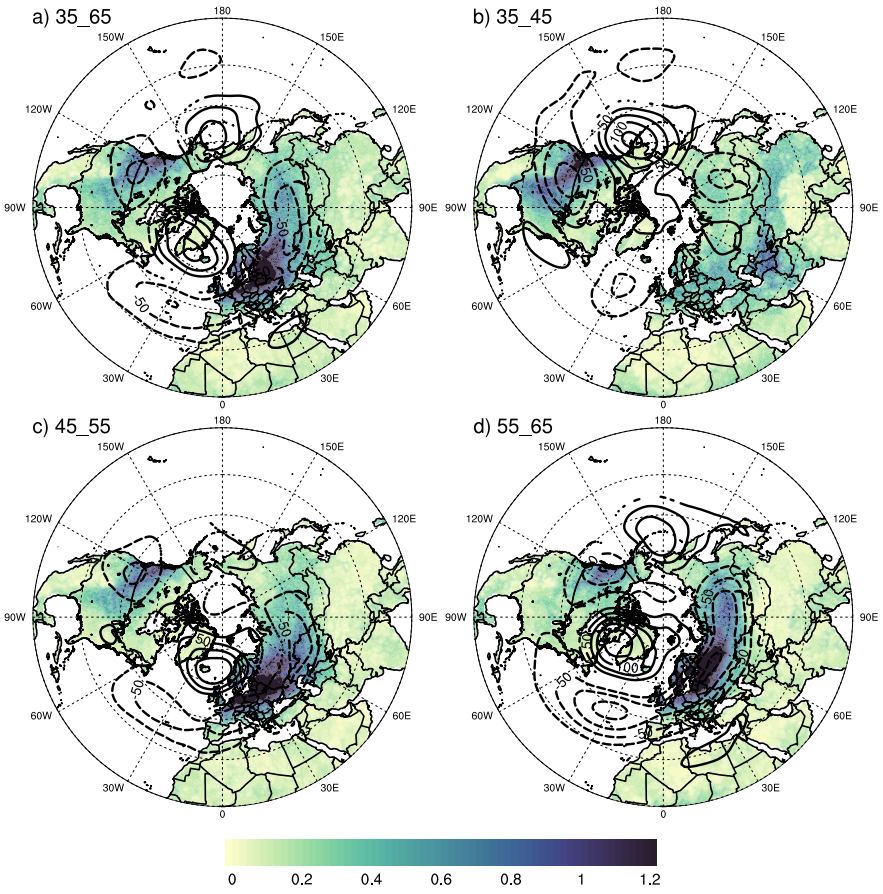

Figure 1. The composite of the geopotential height anomaly relative to climatology (m) at 500 hPa (lines; only significant at the 95% confidence level) and the cold wave magnitude index daily (CWMID; colors) for cold extreme days given by the top 1 % of the MEX over land at the latitude band of a) 35–65°N, b) 35–45°N, c) 45–55°N, and d) 55–65°N.

frequently in some parts of winter. This Monte Carlo test is repeated at least 2000 times to ensure a sufficient sample size, and significant differences from zero are identified at the 95% confidence level.

3 Wave metrics

3.1 Trough and ridge speed

In order to investigate the role of ~~planetary-scale~~ large-scale waves, a Fourier decomposition of ~~geopotential height (gph)~~ gph is employed to separate the field into distinct harmonic waves based on the zonal wave number. The combination of the first five waves is regarded as an estimation of ~~planetary-scale~~ large-scale waves (Z1–5; solid line in Fig. ~~1a)~~3a); these are

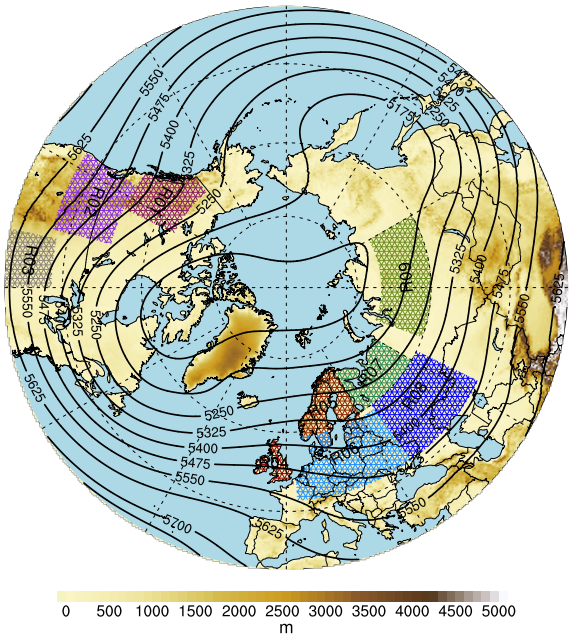

Figure 2. The chosen study regions (hatches). The winter climatology mean geopotential height field (m) and the elevation above mean sea level (m) are shown by contours and shading, respectively.

planetary or Rossby waves (except possibly at high latitudes, where it may be argued that their wave length are too short for the categorization as planetary waves). We estimate the speed of ~~planetary~~ atmospheric wave zonal propagation by utilizing a ~~top-ridge and bottom-trough~~ ridge and trough tracking algorithm (Fig. ~~1~~3a). Small amplitude ridges and troughs are ignored since they are often short lived (red stars in Fig. ~~1~~3a). This is accomplished by considering a threshold for the gph at each local maximum (ridge) and local minimum (trough): At each time step (3-hourly) and latitude, the gph at the ridge (trough) position must be greater (less) than the gph ~~of~~ at 30~~degrees~~ ° to the west and east of the ridge (trough) position ~~plus (minus)~~ by at least 8 % of the Z1–5 amplitude (see blue texts and arrows in Fig. ~~1~~3a). The Z1–5 amplitude is defined as the difference between the highest ridge and the lowest trough at all longitudes around a latitude circle at each time step and latitude. These criteria were carefully chosen after multiple experiments to ensure that all large waves are tracked while minor waves are neglected. Nonetheless, in all the experiments, as long as the thresholds do not suppress large waves, the drawn overall conclusions regarding wave speed changes remain unchanged for other parameter settings. We track each local ridge and trough in time

over longitudes to find the ridge and trough speed, respectively. Also, we save all local ridge ~~positions (~~latitude and longitude ~~: RPLL~~(RLL) and trough ~~positions (TPLL) .~~ (TLL) positions. At each latitude, ridges and troughs are labeled according to their positions (longitude) and are tracked to the next time step by searching for the nearest ridge or trough within a 12-degree limit both to the west and east of their location (Fig. 3b). If no corresponding feature is detected within this range, the ridge or trough is considered to have decayed. Conversely, if a new ridge or trough appears without a corresponding feature in the previous time step, it is considered to have formed.

Note that the ridge and trough speeds as defined here are not the same as the phase or the group speed. Phase speed represents the speed of individual wave numbers, whereas the group velocity is the propagation of the wave «envelope». These are both different from the trough and ridge velocity of combined waves as investigated here. Consequently, here we will refer to the examined velocity simply as the wave speed or the speed of ridges and troughs, intentionally avoiding the terms phase speed or group speed.

3.2 ~~Wave amplitude~~

~~To examine variations in the geopotential field's waviness ,~~ Fig. 4 displays the probability of the winter climatological positions of ridges and troughs, as well as the decay and formation of these features. Most often three major ridges and three major troughs can be seen throughout winters (Fig. 4 and supplementary Fig. S4). The three main ridges are located over the west coast of North America (hereafter, WNA ridge), the western flank of the Tibetan Plateau (hereafter, TP ridge), and the North Atlantic Ocean (hereafter, NAO ridge, at low latitude over the middle part, and at high latitude over the eastern part of the ocean). The three main troughs are located over Eastern North America (hereafter, ENA trough), the eastern Mediterranean (hereafter, EMed trough), and East Asia (hereafter, EAsia trough). The daily speed of these six major ridges and troughs is determined by summing their 3-hourly values across their respective longitudinal ranges (Fig. 3c). The speeds of the ridges over 180°W–90°W, 60°W–30°E, and 30°E–120°E are added to calculate the daily speeds of the WNA ridge, the NAO ridge, and the TP ridge, respectively. The daily speeds of the ENA trough, EMed trough, and EAsia trough are also found by taking the sum of the speeds of the troughs over 120°W–30°W, 0°E–90°E, and 90°E–180°E, respectively (Fig. 3c).

Ridges and troughs typically form upstream of their climatological positions and decay downstream of them (Fig. 4). The WNA ridge, NAO ridge, and ENA trough exhibit stronger formation and decay at high latitudes compared to mid-latitudes, indicating that these ridges and troughs tend to persist longer in the midlatitudes. The TP ridge and EMed trough show large formation and decay at mid-latitudes, likely due to their interaction with the complex orography. Nonetheless, the likelihood of their decay and formation remains significantly lower than their climatological existence, indicating persistency of the ridges and troughs (Fig. 4). The EAsia trough forms more strongly at midlatitudes, while its decay is more pronounced at higher latitudes. Over the Pacific Ocean, there is one ridge and one trough formation center, both of which decay downstream from their formation center. As can be seen from the climatological position of ridges and troughs, there is no strong ridge or trough in these locations, suggesting that these features are short-lived."

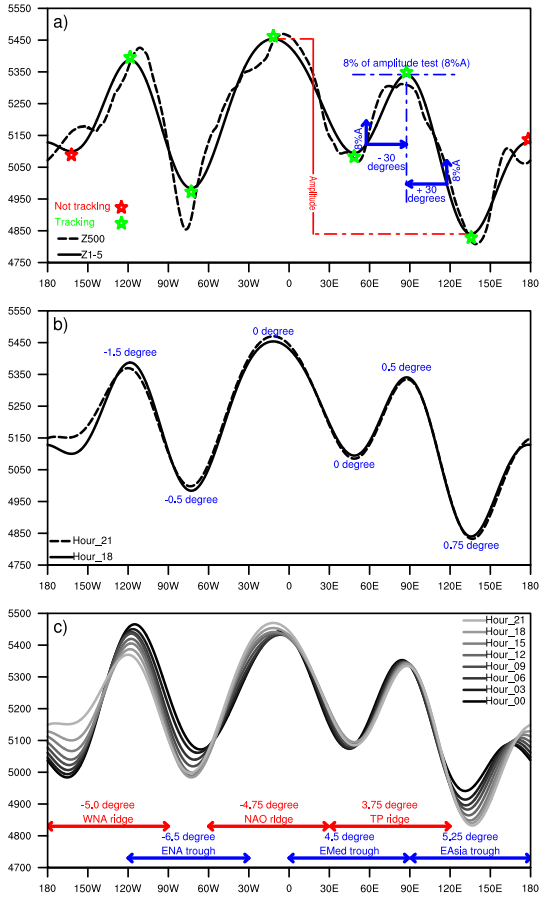

Figure 3. The 500 hPa geopotential height field (Z500; dashed, black line) and the sum of the first five zonal Fourier-decomposed waves of Z500 (Z1–5; solid, black line) for a randomly selected time step (January 7, 2003) at 60°N. The blue text and arrows are associated with a threshold metric that identifies the strength of the ridges and troughs (see method for more information). Based on this threshold, three ridges and three troughs (green stars) are high and deep enough, respectively, for being detected by the tracking algorithm. In this time step, the tracking algorithm will ignore one ridge and one trough (red stars) that do not meet this threshold. b) The Z1–5 for two consecutive time steps (3 hours) and the changes in the ridges' and troughs' longitudinal location between these time steps. c) The Z1–5 for one day (8 time steps) and the calculated longitudinal shifts of each ridge and trough over the entire day.

3.2 Trough and ridge amplitude

Several metrics have been developed to study the waviness of the atmosphere (e.g., Francis and Vavrus, 2012; Barnes, 2013; Hassanzadeh e , many of which rely on the meandering of the ~~meridional extent of a given isohypse (line~~ 500 hPa isohypses (lines of constant gph) ~~is calculated by subtracting the~~ as a proxy. Considering the variations of wave amplitude with different isohypses—e.g., associated with the seasonal variability and poleward shift due to global warming (Barnes, 2013)—selecting an appropriate

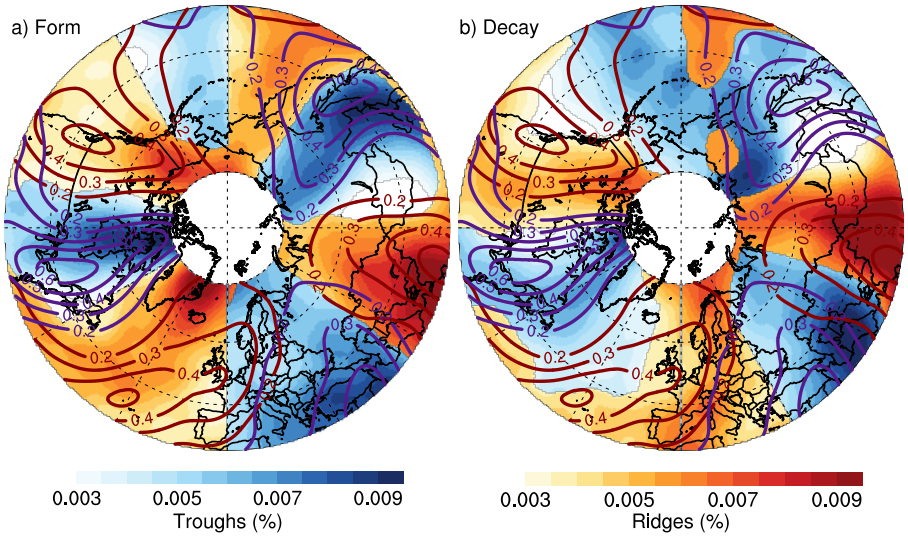

Figure 4. The probability of ridges and troughs and their formation and decay as a function of location. Shown with contours are the probability (in percentage) of 300 hPa ridges (brown) and troughs (purple) during winter climatology as a function of location. The red (blue) shading indicates the climatological probability a) formation and b) decay of ridges (troughs) as a function of location. To show both ridges and troughs in a single plot, priority is given to the stronger feature. A Gaussian function, using a weighted running average over eight degrees in latitude and over an equal distance in longitude, is used to smooth the probabilities.

isohypses are critical. To address these challenges, Cattiaux et al. (2016) derived isohypses from the daily average of the gph at 500 hPa between 30°N and 70°N, hereby varying in time. They regarded the meandering of these isohypses as an indicator of the waviness of the atmospheric flow at 50°N.

Here we focus on identifying changes in waviness at each latitude and at 300, 500, and 850 hPa, which requires some modification of the Cattiaux et al. (2016) approach: For a given study region, the most common isohypse at each time step and latitude is taken as the zonal average of the gph over half of the hemisphere centered on the center longitude of each study region. Then, the meridional wave extent for that latitude is defined as the meridional extent of the associated isohypse determined by calculating the difference between the maximum latitudinal location ~~from~~ and the minimum location of ~~each~~

~~isohypse~~ that isohypse (total gph isohypse extent; TIE). By focusing on half of the hemisphere, it is ensured that at least one full ridge and trough are included within the region. In a similar way, the meridional extent of the first five Fourier decomposition wave numbers of gph (Z1-5) is calculated (planetary isohypse extent; PIE). During cold spells in the defined regions, both TIE and PIE demonstrate the same significant pattern of changes (not shown). This shows the modest impact of small waves on the wave amplitude changes during cold spells. Therefore, we only consider the results of the meridional extent of Z1-5. ~~However, due to the chaotic nature of the gph field, this method will, in some cases,~~

Some isohypses have unconnected subparts (see Fig. 5a), referred to as cut-off low and cut-off high, which might lead to interpretation errors ~~of~~ in the wave amplitude~~(see the supplementary information). We therefore refine the method to solve most of these interpretation ambiguities (see the supplementary information for a description of a refinement of~~. For instance, in Fig. 5a, at high latitudes (around 85°N), the most common isohypse is 8300 m, and at these latitudes, the waviness of this isohypse is small. But, due to a cut-off low of this isohypse at midlatitudes, the estimated wave amplitude at 85°N is large. Moreover, the PIE does not specify the separate contribution to the wave amplitude from ridges and troughs. Understanding these contributions is critical, especially during cold spells, as it helps determine which parts of the wave—ridge or trough—having the greater impact.

Hence, we here propose an alternative metric where the ~~method and for examples of ambiguous gph fields). At a given pressure level, our developed metric provides the~~ meridional extent of the ~~Z1–5 ridges at the latitude and longitude location of its vertical extremes, RPLL.~~ Z1-5 ridges and troughs are measured separately (Fig. 5b). The meridional extent of the ridge is given as the latitudinal difference between the ~~RPLL~~ RLL and the isohypse determined by the zonal average of the Z1–5 over a 90-degree longitude range centered at the ~~RPLL~~ RLL (Fig. ~~1band supplementary Fig. S3b). Hence~~5b, red line); hence, the meridional extent of a ridge at a given latitude is obtained as the difference between that latitude and the latitude of the first cross of the isohypse when moving northward ~~at~~ along the longitude of the ~~RPLL~~RLL. The employed method does not take into account the possible meridional tilting of waves. To address this, at 300 hPa, the wave amplitude is calculated for all longitudes within the 90-degree longitude range. The highest value obtained is then considered the meridional amplitude of the ridge. While the highest value often yields slightly larger wave amplitudes than that ~~at the RPLL~~obtained at the RLL, the overall conclusions regarding changes in wave amplitude during cold spells remain the same for both approaches (not shown). Therefore, to reduce computational usage, we used the amplitude at the ridge position. The meridional extent of troughs ~~is~~ are obtained in a similar way but moving southward from ~~TPLL~~TLL.

The estimated ~~value of wave amplitude~~ meridional amplitudes of a given ridge (trough) is highly influenced by the longitudinal range over which the zonal average of the Z1–5 is taken for determining the isohypse. Using a smaller longitude range yields an isohypse value closer to the value of ~~the gph at RPLL (TPLL). This~~ Z1-5 at RLL (TLL), whici can lead to small ~~wave amplitude values~~amplitudes. Using a large longitude range might yield an isohypse that cannot be found near the ~~RPLL (TPLL~~RLL (TLL), resulting in a missing value for the amplitude. Therefore, after conducting multiple experiments, the 90-degree threshold is chosen. Nonetheless, despite the arbitrariness of the meridional wave amplitude when defined this way, its magnitude ~~remains consistent across latitudes and between~~ exhibits a consistent latitude-dependent pattern and comparable bands of significance in both the climatology and cold-spell cases, which is important and sufficient for this study.

3.3 ~~Significant test~~

~~To test the null hypothesis that anomalies associated with the cold spells are zero, a Monte Carlo simulation with random samples is employed. Specifically,~~ To compare the results of the refined method with PIE, considering the total wave amplitude, the average of the ~~average number of cold spell days across each region is compared with the average of an equivalent number of randomly selected days. Instead of selecting random days from the entire winter season, the selection is weighted based on the frequency distribution through the season of cold spell days, since cold spellsappear to occur more frequently in some parts of winter. This Monte Carlo test is repeated at least 2000 times to ensure a sufficient sample size, and significant differences from zero are identified at the 95% confidence level~~amplitude of the ridges plus those of the troughs over half of the hemisphere centered at each study region is calculated (ridge-trough isohypse extent; RTIE). For climatology, the RTIE amplitude (supplementary Fig. S2, gold lines) is nearly half of the PIE amplitude. During cold spells, there are likewise many similarities between the RTIE and the PIE, yet they have some important differences. During cold spells, the PIE amplifies over a wider latitude range compared to the RTIE. This could be attributed to the influence of cut-off lows or cut-off highs on the amplitude of distant locations.

4 Results

4.1 Wave location

To investigate the impact of planetary waves on the formation of winter cold spells, nine regions with a high likelihood of cold spells are selected (Fig. 2). These regions are chosen based on their significant contribution to the historical extreme cold days on a hemispheric scale (see ~~the supplementary information). In all the study regions, except Northern Siberia, cold days typically coincide with an upstream~~ methodology section). During cold spells over North America (R01, R02, and R03), large-scale gph anomaly patterns show an anticyclonic gph anomaly ~~and a downstream~~ over the North Pacific and a cyclonic gph anomaly over North America (supplementary Fig. ~~S2). It has been demonstrated that northern hemisphere extratropic cold spellsare generally established by northerly cold advection (??), indicating that both cyclonic and anticyclonic gph anomalies play a role in transporting cold air masses from higher latitudes to areas developing and undergoing cold spells.~~

~~Fig. 2 displays the probability for the positions of ridges and troughs for winter climatology. Most often three major ridges and three major troughs can be seen throughout winters~~ S3a, b, and c), similar to the findings of other studies (e.g., Xie et al., 2017) . During cold spells, the locations of the WNA ridge and the ENA trough shift to the west of their corresponding climatological positions (Fig. ~~2 and supplementary Fig. S5). The three main ridges are located over the west coast of North America (hereafter, WNA ridge~~6a, b, and c). This shift is more pronounced for R02 and R03. The NAO ridge extends from northwest Africa to northwest Europe, specifically exhibiting an eastward shift at lower latitudes. For cold spells over western regions of Europe (R04, R05, and R06), the ~~western flank of the Tibetan Plateau (hereafter, TP ridge), and the North Atlantic Ocean (hereafter, NAO ridge, at low latitude over the middle part, and at high latitude over the eastern part of the ocean). The three main troughs are located over Eastern North America (hereafter, ENA trough~~gph anomaly at 500 hPa shows a positive anomaly located north

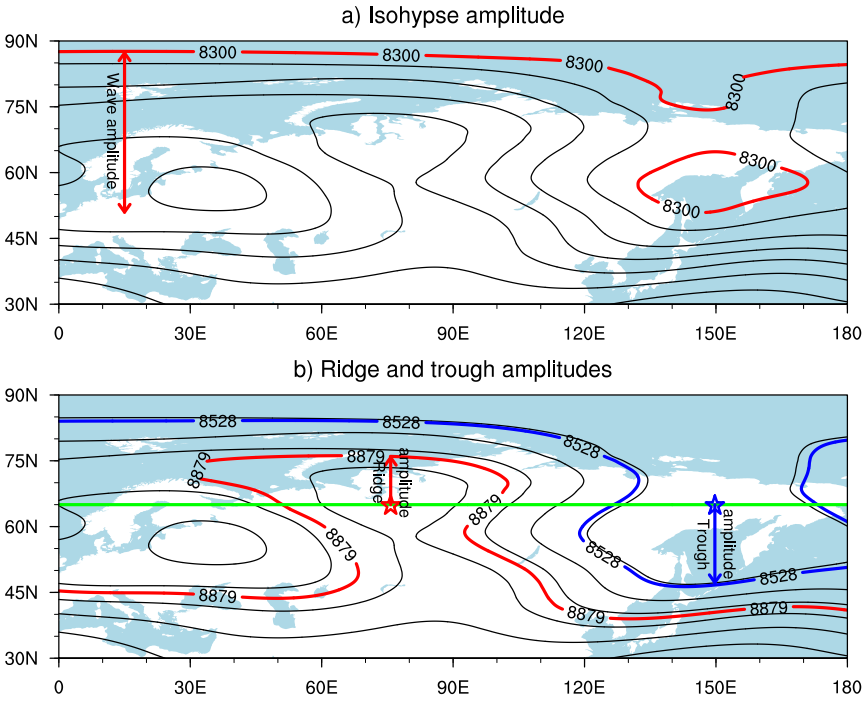

Figure 5. ~~a)~~ The ~~500 hPa geopotential height field (Z500; dashed, black line) and the~~ sum of the first five zonal Fourier-decomposed waves of ~~Z500~~ the 300 hPa geopotential height field (~~Z1–5; solid, black line~~Z1-5) for a randomly selected 3-hourly time step (January 4, 2016, at 18:00). a) The ~~blue text~~ 8300 isohypse and ~~arrows~~ its amplitude are ~~associated with a threshold metric that identifies the strength of the ridges and troughs~~ highlighted; b) The ridge (~~see method for more information~~red arrow) ~~. Based on this threshold, three ridges~~ and ~~three troughs~~ trough (~~green stars~~blue arrow) ~~are high and deep enough, respectively, for being detected by~~ meridional amplitudes at the ~~tracking algorithm. In this time step, the tracking algorithm will ignore one~~ ridge (red star) and ~~one~~ trough (~~red stars~~blue star) ~~that do not meet this threshold. b~~center at latitude 65°N (green line)~~Schematic of ridge~~ . The 8879 isohypse (red ~~arrow~~line) and ~~trough~~ the 8528 isohypse (blue ~~arrow~~line) ~~meridional amplitudes~~are determined by the zonal average of the Z1-5 over a 90-degree longitude range centered at the ridge and trough positions, respectively, at 65°N.

of a negative anomaly (supplementary Fig. S3d, e, and f). This anomaly resembles a high-over-low North Atlantic blocking situation, which is similar to the findings of other studies (e.g., Trigo et al., 2004; Buehler et al., 2011; Pfahl, 2014). For R04 and R05, at high latitudes, the locations of the NAO ridge and EMed trough tend to shift toward the west of their respective climatological centers (Fig. 6d and e). During cold spells over eastern Europe (R08), the ~~eastern Mediterranean (hereafter, EMed trough), and East Asia (hereafter, EAsia trough~~positions of the EMed trough and the TP ridge at high latitudes shift toward the east of their respective climatological locations (Fig. 6h). The ~~location of the WNA ridge, TP ridge, ENA trough , and EAsia trough are mainly determined by large mountain ranges, which force a westerly flow to ascend and move northward~~

along their western slopes, creating a ridge, and descend and move southward on the leeward side, developing a trough (??) . In addition, cold spell over Northern Siberia (R09) primarily aligns with a deep trough downstream over northwest Asia, as depicted in the supplementary Fig. S3i and Fig. 6i. Despite the high latitude of this region, it is sufficiently far from the pole to become affected by cold advection from higher latitudes during cold spells (Tuel and Martius, 2024). For R09 (Fig. 6i), ridges form over the western flank of the Ural Mountains, and the intrinsic relationship between relative and planetary vorticity (that the potential vorticity is almost conserved) implies that mountains cause the zonal air stream to move meridionally and thereby initiate waves in the mid-latitudes (?).

During cold spells, location of the EAsia trough at high latitudes shifts toward the west of its climatological location. These findings indicate that a distinct shifting pattern of ridges and troughs occurs on a hemispheric scale occurs during cold spells over each region(see the supplementary information for details) . Before the onset of cold spells (Fig. 3a, b), upstream ridges encompass . These shifts can also be observed at 500 hPa (not shown) and 850 hPa (not shown), indicating that during cold spells the entire troposphere is shifting in a rather barotropic manner. These shifting patterns suggest an interaction between atmospheric dynamics and surface temperatures.

Fig. 7 shows the retrograding patterns of ridges and troughs before and during cold spells for the composites of regions in North America and Europe. This choice is based on the similarity of the upstream ridge and downstream trough in the selected regions for each composite. In North America, cold spell regions are predominantly located in the vicinity of the WNA ridge. In North America, before cold spells occur, the ridge encompasses a broad area, including the cold-spell region, while downstream troughs are located outside. regions (Fig. 7a). At the start of cold spells, upstream ridges shift to be located outside the upstream ridge becomes more localized in the western side of the cold-spell region, while downstream troughs are now found inside regions (Fig. 3c7e). This configuration enhances the pattern provides northerly wind flow from the Arctic toward the cold-spell location, potentially advecting cold air into the region (see area (supplementary Fig. S6). These findings highlight the critical role of the nearest upstream ridge and downstream trough in the formation of cold spells.

The probability (in percentage) of the position of 300 hPa ridges (red contours) and troughs (blue contours) during winter climatology. The contours indicate probabilities of vertical extremes in latitude and longitude. The hatches indicate the chosen regions for the study on cold spells. A Gaussian function, using a weighted running average over eight degrees in latitude and over an equal distance in longitude, is used to smooth the probabilities. Shading shows the elevation above mean sea level (m).

The probability (in percentage) of the position of 300 hPa ridges (red shading) and troughs (blue shading) for different time lags averaged over all cold spells and all study regions relative to the center of the cold-spell region. The shading indicates probabilities of vertical extremes in latitude and longitude. As the probabilities of ridges and troughs are computed individually, shading of the two fields are shown for values greater than 0.2% to minimize overlap in the plot. Dots indicate regions where cold spells and climatology are significantly different at the 95% confidence level. The green box shows the average latitude and longitude span of all cold spell regions. A Gaussian function, using a weighted running average over eight degrees in latitude and over an equal distance in longitude, is used to smooth the probabilities. a) 20 days ahead of the starting cold spells, b) 10 days ahead of the starting cold spells, c) cold spell starting days, and d) 10 days after the start of cold spells.

4.2 ~~Wave amplitude and speed~~

~~Several studies link the increased likelihood of cold temperature extremes in mid-latitudes to increased upper-atmosphere waviness (e.g., ?). Some studies link extreme cold temperatures to a significant amplified circumglobal waviness based on wave amplitudes of individual wave numbers (??), while others assert a robust correlation between local waviness and cold temperature extremes (??). Local waviness metrics, such as the Rossby wave packet amplitude, combine the ridge and trough into a single unit; therefore, it is unclear how these wave features individually contribute to the amplitude. Previous studies have also shown that the speed of atmospheric waves significantly contributes to cold extreme temperatures in mid-latitudes (e.g., ??) . Slower wave phase speed has been linked to more persistent weather in which extreme cold temperatures can develop, such as atmospheric blocking (?)~~S4). In Europe, most of the cold spell regions are primarily located in the vicinity of the EMed trough. Similar to North America, before cold spells occur, the ridge encompasses a wide area (Fig. 7b), indicating that cold or warm anomalies are not concentrated to specific locations. However, ~~these studies do not establish the role of each ridge and trough in cold spells , and further research is needed to understand how individual wave features interact to influence temperature extremes. Here, we aim to explore the linkage between cold spells and the amplitude and speed of each ridge and trough (see the supplementary and the method sections for details).~~

~~Given the location of ridges and troughs at 300 hPa~~ with the onset of cold spells (Fig. 7f), ridges and troughs become more concentrated, with a ridge positioned upstream and a trough located within the cold-spell regions (Fig. ~~2)~~7f). Hence, associated with cold spells, roughly the same type of regional-scale circulation pattern is found in both North America and Europe. These findings highlight the critical role of the nearest upstream ridge and ~~500 hPa (supplementary Fig. S5), the longitudinal average of the wave amplitudes and speeds for the climatology and cold spellsis calculated in three longitude bands: the amplitudes and speeds of the ridges over 180°W–90°W, 60°W–30°E, and 30°E–120°E are averaged to calculate the amplitudes and speeds of the WNA ridge , the NAO ridge, and the TP ridge, respectively. The amplitudes and speeds of the ENA trough , EMed trough, and EAsia trough are also found by taking the average of the amplitudes and speeds of the troughs over 120°W–30°W, 0°E–90°E, and 90°E–150°W, respectively~~downstream trough in the formation of cold spells.

4.2 Trough and ridge amplitude and speed

For cold spells, the largest ridge and trough amplitude and speed differences relative to climatology occur for the local upstream ridge and downstream trough (supplementary Figs. ~~S7 and S8~~S5 and S6). Generally, the amplitude and speed differences of ridges and troughs decay as their distance increases to the location of the cold spell. A composite over all cold spells and regions of the upstream ridges and downstream troughs provides a general overview of the local wave behavior during cold spells (Fig. ~~4~~8). The upstream ridge significantly amplifies (Fig. ~~4~~8a and supplementary Fig. ~~S7~~S5), facilitating the transfer of Arctic cold air to the cold spell region. ~~The amplification of this ridge also implies the development of higher gph values (warmer air) at higher latitudes, as is also evident in the supplementary Fig. S2.~~ During cold spells, the northward winds entering the Arctic are increasing west of the upstream ridge, while the southward winds exiting the Arctic are increasing east of the upstream ridge (supplementary Fig. ~~S6~~S4). The upstream ridge also significantly slows down (Fig. ~~4~~8b and supplementary Fig. ~~S8~~S6),

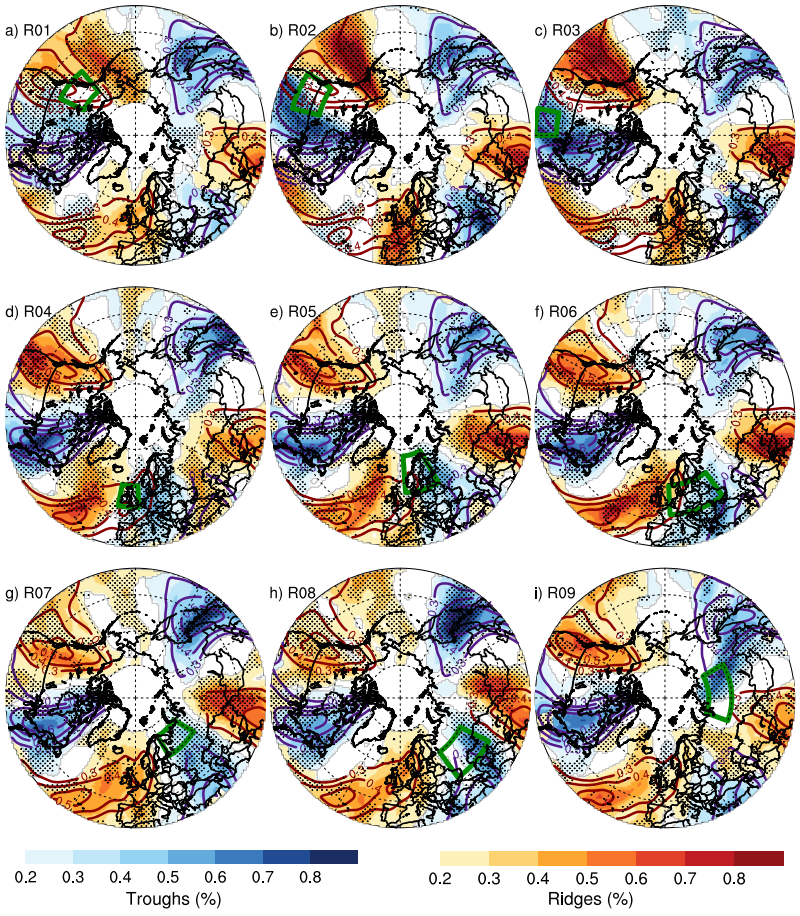

Figure 6. The probability of ridges and troughs at 300 hPa as a function of latitude and longitude. The shading (based on all-time steps of the cold spells) and contours (climatology) indicate probabilities of ridges and troughs in percentage. Solid brown (purple) contours represent the climatological probability of ridges (troughs). Red (blue) shading represents the probability of ridges (troughs) during cold spells over each region. As the probability of ridges and troughs are computed individually, shading and contours of the two fields are shown for values greater than 0.2% to minimize overlap in the plot. Dots indicate regions where cold spells and climatology are significantly different at the 95% confidence level. The green box in each plot shows the location of cold spells. A Gaussian function, using a weighted running average over eight degrees in latitude and over an equal distance in longitude, is used to smooth the probabilities. a) Northwest Canada; b) Northwest US and Southwest Canada; c) Central US; d) British Isles; e) Scandinavia; f) Europe; g) Northwest Russia; h) Southwest Russia; and i) Northern Siberia.

implying the persistence of the warm northward wind to the Arctic and the cold southward wind to the cold spell location. The persistent warm northward wind to the Arctic might be the reason behind the correlation between cold events and a warmer Arctic found in the other studies ~~(e.g., ?)~~(e.g., Cohen et al., 2018); yet more research is needed to discover the impact of the amplified ridge on Arctic temperatures. At low latitudes, the upstream ridge moves faster, which mainly results from cold spells

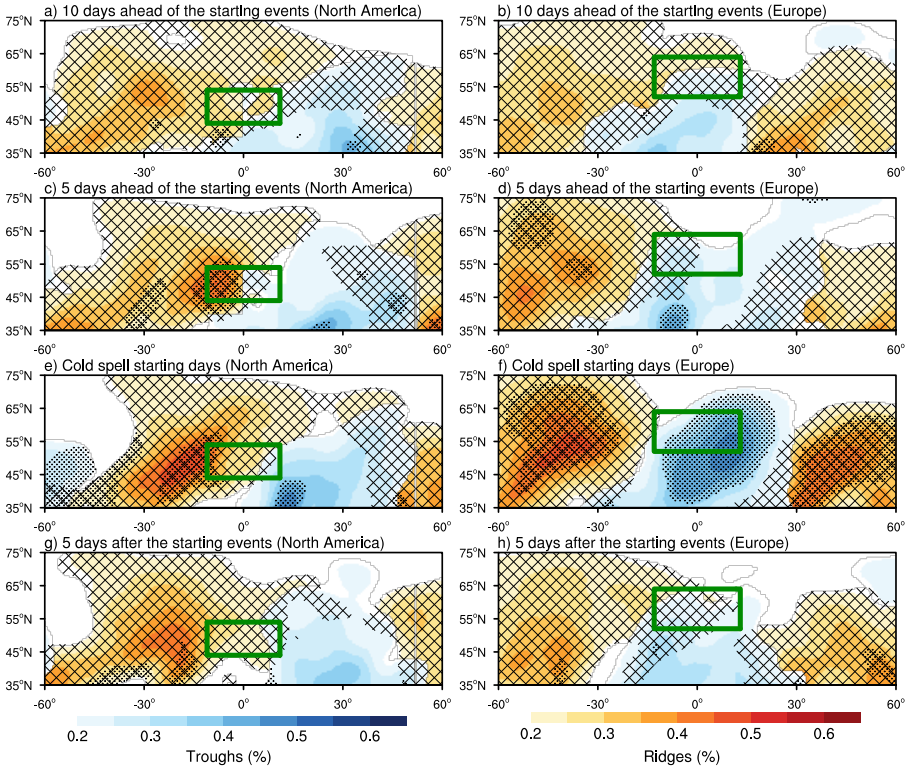

Figure 7. The probability of ridges and troughs at 300 hPa as a function of location and time relative to the start of the cold-spell events. Shown with shading are probabilities (in percentage) of ridges (red) and troughs (blue) for different time lags averaged over all cold spells in study regions relative to the center of the cold-spell region. The panels on the left correspond to the composite of cold spells in North America (R01, R02, and R03), and the panels on the right correspond to the composite of cold spells in Europe (R04, R05, R06, R07, and R08). To show both ridges and troughs in a single plot, priority is given to the stronger feature. The hatched areas represent grid points where ridges are occurring, and dots indicate regions where ridges and troughs during cold spells are significantly different from the climatology at the 95% confidence level. The green box shows the average latitude and longitude span of the cold spell regions. A Gaussian function, using a weighted running average over eight degrees in latitude and over an equal distance in longitude, is used to smooth the probabilities. a), b) 10 days ahead of the starting cold spells; c), d) 5 days ahead of the starting cold spells; e), f) cold spell starting days; and g), h) 5 days after the start of cold spells.

in Northern America and northern Siberia (supplementary Fig. S6). The underlying reasons for this pattern can be explored in future research.

The downstream trough amplifies (deepens) at latitudes north of the cold spell location, while it weakens at southerly latitudes (Fig. ~~4~~8a and supplementary Fig. ~~S7~~S5). For the cold-spell regions in the southern as compared to the northern mid-latitudes, the increase in trough amplitude develops more to the south (supplementary Fig. ~~S7~~S5). Amplification of this trough contributes to enhancing the southward cold wind from the Arctic into the cold spell region (supplementary Fig. ~~S6~~S4). Similar to the upstream ridge, the downstream trough significantly slows down (Fig. ~~4~~8b and supplementary Fig. ~~S8~~S6), hereby increasing the persistency of the cold southward winds into the cold spell region.

~~Climatology (solid lines) and composite of cold spells over all study regions (dashed lines) for a) wave amplitude (degree) and b) wave speed (km day^{-1}) at 300 hPa. Red and blue lines are showing the average of the upstream ridge and the downstream trough, respectively, in the vicinity of each cold spell region. Bold dashed lines indicate difference between cold spell and climatology at the 95% confidence level. The brown box on the left side shows the average latitude span of all regions. A four-degree running average is used to smooth the lines.~~

~~Composites of anomalies relative to climatology of 2-meter temperature, and ridge and trough speed and amplitude during all cold spells as a function of time lag for all study regions. The lag zero (zero on the x-axis) is the day that 30% of the land in each region experiences a cold spell. Blue line is the composite of temperature anomalies averaged over the whole study region. Black and red lines are the composites of ridge and trough amplitude and speed anomalies, respectively. The upstream ridge and the downstream trough in the vicinity of the cold-spell location are shown by solid and dashed lines, respectively. The latitude bands with a significant positive wave amplitude anomaly and a negative wave speed anomaly are averaged for each cold spell region (indicated by the vertical solid lines on the right side of the supplementary Figs. S7 and S8). Bolded solid and bolded dashed lines indicate the difference to climatology significant on a 95% level. a) 300 hPa, b) 500 hPa, and c) 850 hPa.~~

4.3 ~~Causality~~Lead-lag analysis

In the previous section, we have shown that cold spells are associated with higher-amplitude and slowing ridges and troughs in the vicinity of the cold spells. The question that arises is whether cold spells cause the amplification and slowdown of waves or vice versa. Previous research has shown that upper-atmospheric changes—such as amplified planetary waves ~~(?) , blocking (?)~~(Screen and Simmonds, 2014) , blocking (Kautz et al., 2022), and the stratospheric polar vortex ~~(?)~~(Tomassini et al., 2012) —can lead to surface extreme events. ~~Nevertheless, the mechanism by which upper-level changes favor extreme surface weather is not clear.~~ Here, a day-lag analysis of composites over cold spells is provided to shed light on the causal relationship between upper-level waves and surface temperature (Fig. ~~5~~9 and supplementary Fig. ~~S9~~S7). Since the largest wave amplitude and speed differences relative to climatology belong to the upstream ridge and the downstream trough, their time series are plotted here.

The minimum speeds of the upstream ridge and downstream trough occur at a negative time lag several days prior to the onset of the cold spell, which is taken as 30 percent of grid points in the region experiencing a cold spell and indicated by the lag zero. The wave speed anomaly shows almost a similar pattern for both 500 hPa and 300 hPa (Fig. ~~5~~9a and b). This pattern suggests an almost barotropic wave signal through the troposphere during cold spell events. However, the wave-speed reduction occurs somewhat later at 850 hPa, indicating a downward propagation of the wave-speed signal.

Both amplified ridge and trough are also encountered prior to the cold spell, but the speed reduction precedes the amplitude increase (Fig. ~~5~~9a and b). This could potentially be attributed to the breaking of waves due to exceeding the capacity of the wave for the wave activity flux ~~(?)~~(Nakamura and Huang, 2018). The preceding of the upstream ridge and the downstream trough amplification relative to the cold spell suggests that cold spells arise as a result of slow and amplified local upper-atmospheric waves. For Northern Siberia, the downstream trough amplifies at a positive time lag several days after the cold spells (supplementary Fig. S7i), indicating that the amplified trough cannot be responsible for the cold spell in this region. This is consistent with the formation of cold spells in Northern Siberia being due to diabatic processes (Röthlisberger and Papritz, 2023). Nonetheless, the upstream ridge amplifies and slows down prior to the onset of cold spells in this region (supplementary Fig. S7i).

The upstream ridge maximizes simultaneously at all three levels, while the downstream trough amplifies almost simultaneously at 500 and 300 hPa and one day later at 850 hPa. This indicates that during cold spells, the upstream ridge amplification is barotropic, whereas in the lower troposphere, the downstream trough amplification is somewhat baroclinic. It has been shown that during cold spells over China, the positive gph anomaly has a barotropic structure and the negative gph anomaly has a baroclinic structure in the lower troposphere ~~(?)~~(Zhang et al., 2021).

There is no indication that the upstream ridge anomaly is encountered prior to the downstream trough anomaly or vice versa. This suggests that the anomalies could emerge independently in both the ridge and the trough. For instance, in January 2014, poleward low potential vorticity from subtropical deep convection amplified the WNA ridge, while equatorward and downward high potential vorticity deepened the ENA trough ~~(?). ?~~ (Davies, 2015). Li et al. (2017) also showed that only the breakdown of the stratospheric polar vortex cannot be a reliable predictor of cold spells in North America, and warm sea surface temperature in the eastern extratropical Pacific also needs to be considered.

The lead-lag behavior of other significant and non-significant changes in the upstream ridge and downstream trough (supplementary Figs. S5 and S6) is also analyzed. Their time lag either shows no significant changes or occurs after the upstream ridge and downstream trough's significantly positive amplitude and negative speed anomalies (not shown). However, there are some exceptions: During cold spells over North America (R01, R02, and R03), the lead-lag behavior of the upstream ridge anomaly at the lower midlatitudes (35N-50N) indicates that this ridge slows down at these latitudes before it does at other latitudes (supplementary Figs. S8a). For both Eastern European regions (R07 and R08), latitudes with a reduction in the upstream ridge amplitude (35N-40N; supplementary Fig. S7g and h) show strong negative amplitude anomalies weeks before the onset of the cold spell (supplementary Figs. S8b). This indicates that the ridge at lower latitudes tends to move zonally, which may weaken the mixing of warm tropical air with colder midlatitude air long in advance of the cold spell formation."

5 Conclusions

The present study provides a ~~large-scale perspective of changes in Rossby waves during cold spells . Here we show that~~ comprehensive perspective on the formation of cold spells in the midlatitudes, demonstrating that increased wave amplitude and decreased speed are fundamental drivers of cold-spell development. Across all midlatitude regions, locally amplified and

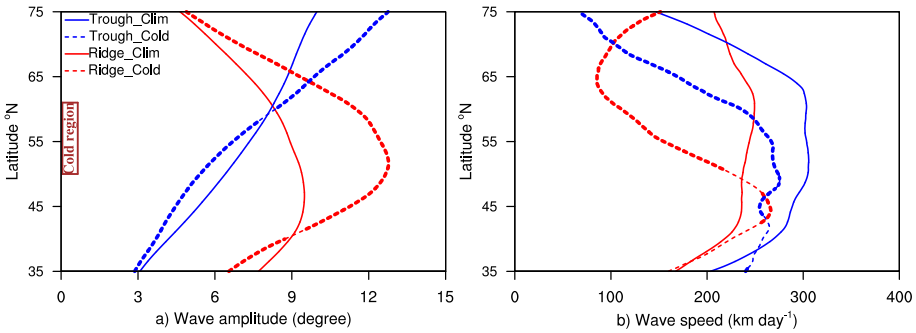

Figure 8. Climatology (solid lines) and composite of cold spells over all study regions (dashed lines) for a) wave amplitude (degree) and b) wave speed ($km\,day^{-1}$) at 300 hPa. Red and blue lines are showing the average of the upstream ridge and the downstream trough, respectively, in the vicinity of each cold spell region. Bold dashed lines indicate difference between cold spell and climatology at the 95% confidence level. The brown box on the left side shows the average latitude span of all regions. A four-degree running average is used to smooth the lines.

slowing ~~Rossby waves in the vicinity of cold spells are favoring the advection of Arctic cold air into the cold-spell region~~ridges and troughs near cold spells appear important for the formation of these. Through a daily lag analysis, a cause-and-effect relationship between upper-level waves and extreme cold surface temperatures is revealed, indicating that upper-level waves are preceding cold spells and hence important for the development of these. Our findings support previous research conducted in a specific region, indicating that slow ~~(e.g., ?) and amplified (e.g., ?)~~ (e.g., Fragkoulidis et al., 2018; Fragkoulidis and Wirth, 2020) and amplified (e.g., Jolly et al., 2021; Fragkoulidis and Wirth, 2020) Rossby waves contribute to cold spells ~~in~~ Europe. Moreover, we demonstrate the importance of ridge and trough development at each latitude within the mid-latitudes~~.~~, whereas others (e.g., Fragkoulidis and Wirth, 2020) discuss daily averages of speed and amplitude over an area encompassing the cold-spell region. By focusing on latitude rather than averaging over a broader region, we determine that the slow and amplified waves are mostly in the vicinity or north of the cold spell regions.

Additionally, we discuss the importance of wave location in cold spell development, as shifting the location of waves relative to climatology can result in a cold air advection to the cold region. Our findings highlight the critical importance of wave

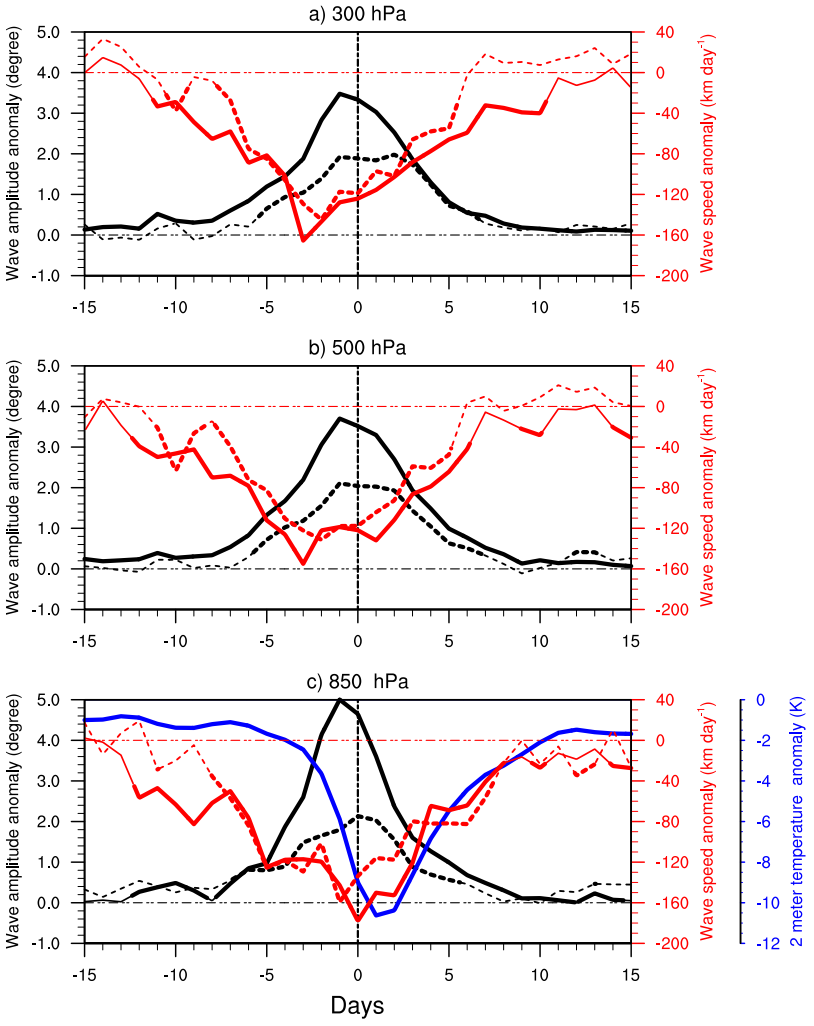

Figure 9. Composites of anomalies relative to climatology of 2-meter temperature, and ridge and trough speed and amplitude during all cold spells as a function of time lag for all study regions. The lag zero (zero on the x-axis) is the day that 30% of the land in each region experiences a cold spell. Blue line is the composite of temperature anomalies averaged over the whole study region. Black and red lines are the composites of ridge and trough amplitude and speed anomalies, respectively. The upstream ridge and the downstream trough in the vicinity of the cold-spell location are shown by solid and dashed lines, respectively. The latitude bands with a significant positive wave amplitude anomaly and a negative wave speed anomaly are averaged for each cold spell region (indicated by the vertical solid lines on the right side of the supplementary Figs. S5 and S6). Bolded solid and bolded dashed lines indicate the difference to climatology significant on a 95% level. a) 300 hPa, b) 500 hPa, and c) 850 hPa.

location, emphasizing the need to consider potential shifts in wave positions in a warming world. Such shifts could result in more frequent extreme events in certain areas, impacting local climates.

It is important to note that this research primarily focused on the nearest ridge and trough relative to the location of cold spells. However, an upper-level anomaly can propagate both downstream and upstream (e.g., Simmons and Hoskins, 1979). Consequently, the anomaly that ultimately triggers the formation of cold spells may initially originate from a remote ridge or trough, and further investigation is required to explore each region in greater depth.

Considering the increasing frequency of heat waves, floods, and droughts due to climate change ~~(IPCC; ?)~~(IPCC; Seneviratne et al., 2021 , there is a need to understand the dynamical drivers of them ~~(?)~~(Xu et al., 2024). In this context, we have developed two tools designed to identify the amplitude and speed of atmospheric waves, which can be utilized in future research to unravel the dynamical drivers of various extreme events. Furthermore, these metrics may help clarify the impact of AA on the waviness and speed of Rossby waves. Our meridional wave amplitude metric provides a unique methodology compared to other metrics (Geen et al., 2023), as it could evaluate changes in ridge and trough independently in a warming world.

Code availability. Codes are available at https://doi.org/10.5281/zenodo.16761350

Data availability. We obtained the ERA5 data from the ECMWF data server on pressure levels at https://cds.climate.copernicus.eu/datasets/reanalysis-era5-pressure-levels?tab=download and single levels at https://cds.climate.copernicus.eu/datasets/reanalysis-era5-single-levels?tab=download.

Author contributions. All authors conceived and designed the study. Material preparation, data collection and analysis were performed by MB. The first draft of the manuscript was written by MB with comments and revisions from RGG and JPS. All authors read and approved the final manuscript.

Competing interests. The authors declare no competing interests.

Acknowledgements. The work is part of the project: The role of atmospheric circulation in extreme weather events, funded by the Faculty of Science and Technology, University of Tromsø. We sincerely thank the handling co-editor, Gwendal Rivière, and the two anonymous reviewers for their valuable feedback, which greatly contributed to the improvement of this study.

References

Barnes, E. A.: Revisiting the evidence linking Arctic amplification to extreme weather in midlatitudes, Geophys. Res. Lett., 40, 4734–4739, https://doi.org/https://doi.org/10.1002/grl.50880, 2013.

Barnes, M. A., King, M., Reeder, M., and Jakob, C.: The dynamics of slow-moving coherent cyclonic potential vorticity anomalies and their links to heavy rainfall over the eastern seaboard of Australia, Q. J. R. Meteorol. Soc., 149, 2233–2251, https://doi.org/https://doi.org/10.1002/qj.4503, 2023.

Barriopedro, D., García-Herrera, R., Lupo, A. R., and Hernández, E.: A Climatology of Northern Hemisphere Blocking, J. Clim., 19, 1042–1063, https://doi.org/10.1175/JCLI3678.1, 2006.

Bieli, M., Pfahl, S., and Wernli, H.: A Lagrangian investigation of hot and cold temperature extremes in Europe, Q. J. R. Meteorol. Soc., 141, 98–108, https://doi.org/10.1002/qj.2339, 2015.

Blackmon, M. L., Lee, Y.-H., Wallace, J. M., and Hsu, H.: Time Variation of 500 mb Height Fluctuations with Long, Intermediate and Short Time Scales as Deduced from Lag-Correlation Statistics, J. Atmos. Sci., 41, 981–991, https://doi.org/10.1175/1520-0469(1984)041<0981:TVOMHF>2.0.CO;2, 1984.

Blackport, R., Fyfe, J. C., and Screen, J. A.: Arctic change reduces risk of cold extremes, Science, 375, 729–729, https://doi.org/10.1126/science.abn2414, 2022.

Blackport, R., Sigmond, M., and Screen, J. A.: Models and observations agree on fewer and milder midlatitude cold extremes even over recent decades of rapid Arctic warming, Sci. Adv., 10, eadp1346, https://doi.org/10.1126/sciadv.adp1346, 2024.

Buehler, T., Raible, C. C., and Stocker, T. F.: The relationship of winter season North Atlantic blocking frequencies to extreme cold or dry spells in the ERA-40, Tellus A: Dyn. Meteorol. Oceanogr., 63, 174–187, https://doi.org/10.1111/j.1600-0870.2010.00492.x, 2011.

Cattiaux, J., Peings, Y., Saint-Martin, D., Trou-Kechout, N., and Vavrus, S. J.: Sinuosity of midlatitude atmospheric flow in a warming world, Geophys. Res. Lett., 43, 8259–8268, https://doi.org/https://doi.org/10.1002/2016GL070309, 2016.

Chen, G., Lu, J., Burrows, D. A., and Leung, L. R.: Local finite-amplitude wave activity as an objective diagnostic of midlatitude extreme weather, Geophys. Res. Lett., 42, https://doi.org/https://doi.org/10.1002/2015GL066959, 2015.

Chen, X. and Luo, D.: Arctic sea ice decline and continental cold anomalies: Upstream and downstream effects of Greenland blocking, Geophys. Res. Lett., 44, 3411–3419, https://doi.org/https://doi.org/10.1002/2016GL072387, 2017.

Cohen, J., Screen, J. A., Furtado, J. C., Barlow, M., Whittleston, D., Coumou, D., and Jones, J.: Recent Arctic amplification and extreme mid-latitude weather, Nat. Geosci., 7, 627–637, https://doi.org/https://doi.org/10.1038/ngeo2234, 2014.

Cohen, J., Pfeiffer, K., and Francis, J. A.: Warm Arctic episodes linked with increased frequency of extreme winter weather in the United States, Nat. Commun., 9, 869, https://doi.org/https://doi.org/10.1038/s41467-018-02992-9, 2018.

Cohen, J., Agel, L., Barlow, M., Garfinkel, C. I., and White, I.: Linking Arctic variability and change with extreme winter weather in the United States, Science, 373, 1116–1121, https://doi.org/10.1126/science.abi9167, 2021.

Cohen, J., Francis, J. A., and Pfeiffer, K.: Anomalous Arctic warming linked with severe winter weather in Northern Hemisphere continents, Commun. Earth Environ., 5, 557, https://doi.org/https://doi.org/10.1038/s43247-024-01720-0, 2024.

Coumou, D., Petoukhov, V., Rahmstorf, S., Petri, S., and Schellnhuber, H. J.: Quasi-resonant circulation regimes and hemispheric synchronization of extreme weather in boreal summer, PNAS, 111, 12 331–12 336, https://doi.org/10.1073/pnas.1412797111, 2014.

Coumou, D., Lehmann, J., and Beckmann, J.: The weakening summer circulation in the Northern Hemisphere mid-latitudes, Science, 348, 324–327, https://doi.org/10.1126/science.1261768, 2015.

Davies, H. C.: Weather chains during the 2013/2014 winter and their significance for seasonal prediction, Nat. Geosci., 8, 833–837, https://doi.org/https://doi.org/10.1038/ngeo2561, 2015.

Domeisen, D. I. V., Martius, O., and Jiménez-Esteve, B.: Rossby Wave Propagation into the Northern Hemisphere Stratosphere: The Role of Zonal Phase Speed, Geophys. Res. Lett., 45, 2064–2071, https://doi.org/10.1002/2017GL076886, 2018.

Fischer, E. M., Sippel, S., and Knutti, R.: Increasing probability of record-shattering climate extremes, Nat. Clim. Chang., 11, 689–695, https://doi.org/https://doi.org/10.1038/s41558-021-01092-9, 2021.

Fragkoulidis, G.: Decadal variability and trends in extratropical Rossby wave packet amplitude, phase, and phase speed, Weather Climate Dyn., 3, 1381–1398, https://doi.org/10.5194/wcd-3-1381-2022, 2022.

Fragkoulidis, G. and Wirth, V.: Local Rossby Wave Packet Amplitude, Phase Speed, and Group Velocity: Seasonal Variability and Their Role in Temperature Extremes, J. Clim., 33, 8767–8787, https://doi.org/10.1175/JCLI-D-19-0377.1, 2020.

Fragkoulidis, G., Wirth, V., Bossmann, P., and Fink, A. H.: Linking Northern Hemisphere temperature extremes to Rossby wave packets, Q. J. R. Meteorol. Soc., 144, 553–566, https://doi.org/https://doi.org/10.1002/qj.3228, 2018.

Francis, J. A. and Vavrus, S. J.: Evidence linking Arctic amplification to extreme weather in mid-latitudes, Geophys. Res. Lett., 39, 2012GL051 000, https://doi.org/https://doi.org/10.1029/2012GL051000, 2012.

Geen, R., Thomson, S. I., Screen, J. A., Blackport, R., Lewis, N. T., Mudhar, R., Seviour, W. J. M., and Vallis, G. K.: An Explanation for the Metric Dependence of the Midlatitude Jet-Waviness Change in Response to Polar Warming, Geophys. Res. Lett., 50, e2023GL105 132, https://doi.org/https://doi.org/10.1029/2023GL105132, 2023.

Hanna, E. and Cropper, T. E.: North Atlantic Oscillation, https://doi.org/10.1093/acrefore/9780190228620.013.22, 2017.

Hassanzadeh, P., Kuang, Z., and Farrell, B. F.: Responses of midlatitude blocks and wave amplitude to changes in the meridional temperature gradient in an idealized dry GCM, Geophys. Res. Lett., 41, 5223–5232, https://doi.org/https://doi.org/10.1002/2014GL060764, 2014.

Hersbach, H., Bell, B., Berrisford, P., Hirahara, S., Horányi, A., Muñoz-Sabater, J., Nicolas, J., Peubey, C., Radu, R., Schepers, D., Simmons, A., Soci, C., Abdalla, S., Abellan, X., Balsamo, G., Bechtold, P., Biavati, G., Bidlot, J., Bonavita, M., De Chiara, G., Dahlgren, P., Dee, D., Diamantakis, M., Dragani, R., Flemming, J., Forbes, R., Fuentes, M., Geer, A., Haimberger, L., Healy, S., Hogan, R. J., Hólm, E., Janisková, M., Keeley, S., Laloyaux, P., Lopez, P., Lupu, C., Radnoti, G., de Rosnay, P., Rozum, I., Vamborg, F., Villaume, S., and Thépaut, J.-N.: The ERA5 global reanalysis, Q. J. R. Meteorol. Soc., 146, 1999–2049, https://doi.org/https://doi.org/10.1002/qj.3803, 2020.

Hoskins, B. and Woollings, T.: Persistent Extratropical Regimes and Climate Extremes, Curr. Climate Change Rep., 1, 115–124, https://doi.org/https://doi.org/10.1007/s40641-015-0020-8, 2015.

Jolly, E., d'Andrea, F., Rivière, G., and Fromang, S.: Linking warm Arctic winters, Rossby waves, and cold spells: an idealized numerical study, J. Atmos. Sci., 78, 2783–2799, https://doi.org/https://doi.org/10.1175/JAS-D-20-0088.1, 2021.

Kautz, L. A., Martius, O., Pfahl, S., Pinto, J. G., Ramos, A. M., Sousa, P. M., and Woollings, T.: Atmospheric blocking and weather extremes over the Euro-Atlantic sector–a review, WCD, 3, 305–336, https://doi.org/10.5194/wcd-3-305-2022, 2022.

Kornhuber, K., Petoukhov, V., Petri, S., Rahmstorf, S., and Coumou, D.: Evidence for wave resonance as a key mechanism for generating high-amplitude quasi-stationary waves in boreal summer, Clim. Dyn., 49, 1961–1979, https://doi.org/10.1007/s00382-016-3399-6, 2017.

Kornhuber, K., Osprey, S., Coumou, D., Petri, S., Petoukhov, V., Rahmstorf, S., and Gray, L.: Extreme weather events in early summer 2018 connected by a recurrent hemispheric wave-7 pattern, Environ. Res. Lett., 14, 054 002, https://doi.org/10.1088/1748-9326/ab13bf, 2019.

Li, Z., Manson, A. H., Li, Y., and Meek, C.: Circulation characteristics of persistent cold spells in central–eastern North America, J. Meteorol. Res., 31, 250–260, https://doi.org/https://doi.org/10.1007/s13351-017-6146-y, 2017.

Morlot, M., Russo, S., Feyen, L., and Formetta, G.: Trends in heat and cold wave risks for the Italian Trentino-Alto Adige region from 1980 to 2018, NHESS, 23, 2593–2606, 2023.

Nakamura, N. and Huang, C. S.: Atmospheric blocking as a traffic jam in the jet stream, Science, 361, 42–47, https://doi.org/10.1126/science.aat0721, 2018.

Petoukhov, V., Rahmstorf, S., Petri, S., and Schellnhuber, H. J.: Quasiresonant amplification of planetary waves and recent Northern Hemisphere weather extremes, PNAS, 110, 5336–5341, https://doi.org/10.1073/pnas.1222000110, 2013.

Pfahl, S.: Characterising the relationship between weather extremes in Europe and synoptic circulation features, NHESS, 14, 1461–1475, https://doi.org/10.5194/nhess-14-1461-2014, 2014.

Pfleiderer, P. and Coumou, D.: Quantification of temperature persistence over the Northern Hemisphere land-area, Clim. Dyn., 51, 627–637, https://doi.org/https://doi.org/10.1007/s00382-017-3945-x, 2018.

Randel, W. J. and Held, I. M.: Phase Speed Spectra of Transient Eddy Fluxes and Critical Layer Absorption, J. Atmos. Sci., 48, 688–697, https://doi.org/10.1175/1520-0469(1991)048<0688:PSSOTE>2.0.CO;2, 1991.

Reid, K. J., Barnes, M. A., Gillett, Z. E., Parker, T., Udy, D. G., Ayat, H., Boschat, G., Bowden, A., Grosfeld, N. H., King, A. D., Richardson, D., Shao, Y., Teckentrup, L., Trewin, B., Hope, P., Zhou, L., Borowiak, A. R., Holgate, C. M., and Isphording, R. N.: A Multiscale Evaluation of the Wet 2022 in Eastern Australia, AMS, 38, 909 – 929, https://doi.org/10.1175/JCLI-D-24-0224.1, 2025.

Ribes, A., Robin, A., Tessiot, A., and Cattiaux, J.: Recent Extreme Cold Waves are Likely Not to Happen Again This Century, Bull. Am. Meteorol. Soc, 106, E1759 – E1771, https://doi.org/10.1175/BAMS-D-24-0013.1, 2025.

Riboldi, J., Lott, F., D'Andrea, F., and Rivière, G.: On the Linkage Between Rossby Wave Phase Speed, Atmospheric Blocking, and Arctic Amplification, Geophys. Res. Lett., 47, e2020GL087 796, https://doi.org/https://doi.org/10.1029/2020GL087796, 2020.

Röthlisberger, M. and Papritz, L.: A Global Quantification of the Physical Processes Leading to Near-Surface Cold Extremes, Geophys. Res. Lett., 50, e2022GL101 670, https://doi.org/10.1029/2022GL101670, 2023.

Röthlisberger, M., Pfahl, S., and Martius, O.: Regional-scale jet waviness modulates the occurrence of midlatitude weather extremes, Geophys. Res. Lett., 43, 10,989–10,997, https://doi.org/https://doi.org/10.1002/2016GL070944, 2016.

Röthlisberger, M., Frossard, L., Bosart, L. F., Keyser, D., and Martius, O.: Recurrent Synoptic-Scale Rossby Wave Patterns and Their Effect on the Persistence of Cold and Hot Spells, J. Climate, 32, 3207–3226, https://doi.org/10.1175/JCLI-D-18-0664.1, 2019.

Screen, J. A. and Simmonds, I.: Exploring links between Arctic amplification and mid-latitude weather, Geophys. Res. Lett., 40, 959–964, https://doi.org/https://doi.org/10.1002/grl.50174, 2013.

Screen, J. A. and Simmonds, I.: Amplified mid-latitude planetary waves favour particular regional weather extremes, Nat. Clim. Chang., 4, 704–709, https://doi.org/https://doi.org/10.1038/nclimate2271, 2014.

Seneviratne, S. I., Zhang, X., Adnan, M., Badi, W., Dereczynski, C., Luca, A. D., Ghosh, S., Iskandar, I., Kossin, J., Lewis, S., Otto, F., Pinto, I., Satoh, M., Vicente-Serrano, S. M., Wehner, M., Zhou, B., and Allan, R.: Weather and climate extreme events in a changing climate, in: Climate Change 2021: The Physical Science Basis: Working Group I contribution to the Sixth Assessment Report of the Intergovernmental Panel on Climate Change, edited by Masson-Delmotte, V. P., Zhai, A., Pirani, S. L., and Connors, C., pp. 1513–1766, Cambridge University Press, Cambridge, UK, https://doi.org/10.1017/9781009157896.013, 2021.

Simmons, A. J. and Hoskins, B. J.: The Downstream and Upstream Development of Unstable Baroclinic Waves, J. Atmos. Sci., 36, 1239 – 1254, https://doi.org/10.1175/1520-0469(1979)036<1239:TDAUDO>2.0.CO;2, 1979.

Stendel, M., Francis, J., White, R., Williams, P. D., and Woollings, T.: Chapter 15 - The jet stream and climate change, in: Climate Change (Third Edition), edited by Letcher, T. M., pp. 327–357, Elsevier, third edition edn., https://doi.org/https://doi.org/10.1016/B978-0-12-821575-3.00015-3, 2021.

Takaya, K. and Nakamura, H.: A Formulation of a Phase-Independent Wave-Activity Flux for Stationary and Migratory Quasigeostrophic Eddies on a Zonally Varying Basic Flow, J. Atmos. Sci., 58, 608–627, https://doi.org/10.1175/1520-0469(2001)058<0608:AFOAPI>2.0.CO;2, 2001.

Teng, H. and Branstator, G.: Amplification of Waveguide Teleconnections in the Boreal Summer, Curr. Clim. Change Rep., 5, 421–432, https://doi.org/10.1007/s40641-019-00150-x, 2019.

Tomassini, L., Gerber, E. P., Baldwin, M. P., Bunzel, F., and Giorgetta, M.: The role of stratosphere-troposphere coupling in the occurrence of extreme winter cold spells over northern Europe, J. Adv. Model. Earth Syst., 4, https://doi.org/https://doi.org/10.1029/2012MS000177, 2012.

Trigo, R. M., Trigo, I. F., DaCamara, C. C., and Osborn, T. J.: Climate impact of the European winter blocking episodes from the NCEP/NCAR Reanalyses, Clim. Dyn., 23, 17–28, https://doi.org/https://doi.org/10.1007/s00382-004-0410-4, 2004.

Tuel, A. and Martius, O.: Persistent warm and cold spells in the Northern Hemisphere extratropics: regionalisation, synoptic-scale dynamics and temperature budget, WCD, 5, 263–292, https://doi.org/10.5194/wcd-5-263-2024, 2024.

van Mourik, J., de Vries, H., and Baatsen, M.: On the movement of atmospheric blocking systems and the associated temperature responses, WCD, 6, 413–429, https://doi.org/10.5194/wcd-6-413-2025, 2025.

Vihma, T., Graversen, R., Chen, L., Handorf, D., Skific, N., Francis, J. A., Tyrrell, N., Hall, R., Hanna, E., Uotila, P., Dethloff, K., Karpechko, A. Y., Björnsson, H., and Overland, J. E.: Effects of the tropospheric large-scale circulation on European winter temperatures during the period of amplified Arctic warming, Int. J. Climatol., 40, 509–529, https://doi.org/https://doi.org/10.1002/joc.6225, 2020.

Vries, A. J. d., Wicker, W., Fragkoulidis, G., Rudeva, I., Rivoire, P., Russo, E., Casselman, J. W., Yadav, P., Pilon, R., Afargan-Gerstman, H., Nangombe, S., Hart, N. C. G., and Domeisen, D. I. V.: Extreme Weather in the Southern Hemisphere in Early 2022, Bull. Am. Meteorol. Soc., pp. BAMS–D–23–0141.1, https://doi.org/10.1175/BAMS-D-23-0141.1, 2025.

White, R. H., Kornhuber, K., Martius, O., and Wirth, V.: From Atmospheric Waves to Heatwaves: A Waveguide Perspective for Understanding and Predicting Concurrent, Persistent, and Extreme Extratropical Weather, Bull. Am. Meteorol. Soc., 103, E923–E935, https://doi.org/10.1175/BAMS-D-21-0170.1, 2022.

Wicker, W., Harnik, N., Pyrina, M., and Domeisen, D. I.: Heatwave location changes in relation to Rossby wave phase speed, Geophys. Res. Lett., 51, e2024GL108 159, https://doi.org/https://doi.org/10.1029/2024GL108159, 2024.

Xie, Z., Black, R. X., and Deng, Y.: The structure and large-scale organization of extreme cold waves over the conterminous United States, Clim. Dyn., 49, 4075–4088, https://doi.org/https://doi.org/10.1007/s00382-017-3564-6, 2017.

Xu, G., Broadman, E., Dorado-Liñán, I., Klippel, L., Meko, M., Büntgen, U., De Mil, T., Esper, J., Gunnarson, B., Hartl, C., Krusic, P. J., Linderholm, H. W., Ljungqvist, F. C., Ludlow, F., Panayotov, M., Seim, A., Wilson, R., Zamora-Reyes, D., and Trouet, V.: Jet stream controls on European climate and agriculture since 1300 CE, Nature, 634, 600–608, https://doi.org/10.1038/s41586-024-07985-x, 2024.

Yao, Y., Luo, D., Dai, A., and Simmonds, I.: Increased Quasi Stationarity and Persistence of Winter Ural Blocking and Eurasian Extreme Cold Events in Response to Arctic Warming. Part I: Insights from Observational Analyses, J. Climate, 30, 3549 – 3568, https://doi.org/10.1175/JCLI-D-16-0261.1, 2017.

Zhang, L., Xie, Z., Deng, Y., and Huang, W.: Structure and Large-Scale Organization of Extreme Cold Wave Events Over the Chinese Mainland During the Boreal Cold Season, J. Geophys. Res. Atmos., 126, e2021JD035 005, https://doi.org/10.1029/2021JD035005, 2021.

Zschenderlein, P., Fragkoulidis, G., Fink, A. H., and Wirth, V.: Large-scale Rossby wave and synoptic-scale dynamic analyses of the unusually late 2016 heatwave over Europe, Weather, 73, 275–283, https://doi.org/https://doi.org/10.1002/wea.3278, 2018.